

# EarthCARE Cloud Profiling Radar Observations of the Vertical Structure of Marine Stratocumulus Clouds

Zhuocan Xu,<sup>1</sup> Pavlos Kollias,<sup>1,2</sup> Susmitha Sasikumar,<sup>3</sup> Alessandro Battaglia,<sup>3</sup> Bernat Puigdomènech Treserras,<sup>2</sup> and Matthew L. Walker McLinden<sup>4</sup>

5 <sup>1</sup> *Division of Atmospheric Sciences, Stony Brook University, NY USA*

<sup>2</sup> *Department of Atmospheric and Oceanic Sciences, McGill University, Montreal, Canada*

<sup>3</sup> *Department of Environment, Land and Infrastructure Engineering, Politecnico di Torino, Turin, Italy*

<sup>4</sup> *NASA Goddard Space Flight Center, Greenbelt, MD USA*

*Correspondence to: Zhuocan Xu (zhuocan.xu@stonybrook.edu)*

10 **Abstract.** Launched in May 2024, the EarthCARE Cloud Profiling Radar (EC-CPR) provides enhanced sensitivity, finer horizontal resolution, finer vertical sampling and greatly reduced surface clutter contamination compared to its predecessor, the CloudSat's CPR (CS-CPR). These improvements enable more accurate detection and characterization of the vertical structure of marine low-level clouds. This study presents the first year of EC-CPR observations of stratocumulus (Sc) clouds over the Southeast Pacific and Southeast Atlantic Oceans.

15 The analysis of EC-CPR clear-sky profiles and comparisons with airborne radar data confirm that surface clutter is effectively suppressed above 0.5 km. Comparisons with CS-CPR data from 2007–2008 show that EC-CPR detects nearly double the Sc amount relative to CS-CPR in the regions of study. When a columnar maximum reflectivity ( $Z_{MAX}$ ) threshold of  $-15$  dBZ is used to flag raining profiles, CS-CPR is found to underestimate rainfall occurrence by  $\sim 20\%$  for  $Z_{MAX}$  located between 500 and 750 m above the surface.

20 Using a steady-state one-dimensional drizzle model, the impact of the point target response (PTR) on EC-CPR reflectivity profiles in Sc clouds is examined. PTR causes vertical stretching of radar-detected cloud boundaries, resulting in an overestimation of cloud thickness by approximately 0.4–0.5 km in drizzling clouds. Additionally, PTR induces parabolic shaping of reflectivity profiles regardless of drizzle presence, complicating the distinction between drizzle-free and drizzle-containing clouds. These findings underscore the need for cautious interpretation of radar reflectivity profiles and suggest the  
25 incorporation of additional constraints, such as Doppler velocity and path-integrated attenuation to improve future drizzle detection strategies.

## 1 Introduction

Stratocumulus (Sc) clouds cover extensive areas of the subtropical oceans especially near the eastern continental boundaries (Hartmann et al., 1992; Wood, 2012). These extensive low-level clouds exert a strong net cooling radiative effect by strongly  
30 reflecting the incoming shortwave radiation, while having a relatively small impact on outgoing longwave emission due to

their low altitude. Several processes including turbulent mixing, drizzle formation, mesoscale organization active at different scales contribute to their radiative and microphysical properties.

35 Drizzle that may or may not reach the Earth's surface is ubiquitous in the marine Sc (Glienke et al, 2017; Wu et al., 2017, Yang et al., 2017, Zhu et a., 2022). In spite of the low intensity on average ( $0.5$  to  $2$   $\text{mmday}^{-1}$  considered as moderate drizzle, Wood, 2012), the evolution of drizzle has a critical role in shaping the interaction of aerosol, macrophysics, microphysics and dynamics of Sc clouds (e.g., L'Ecuyer et al, 2009; Wood et al., 2012; Yamaguchi et al., 2017; Eastman et al., 2021), which subsequently modulate the overall cloud albedo, lifetime and the effectiveness of associated climate cooling (Mülmenstädt et al., 2021).

40

The National Aeronautics and Space Administration (NASA) CloudSat Cloud Profiling Radar (CS-CPR) lead the pioneering efforts of observing low level stratiform marine clouds and associated light precipitation globally (Stephens et al., 2002). The CS-CPR is the first 94-GHz radar in space with initial sensitivity at around  $-30$  dBZ (Tanelli et al., 2008). The reflectivity was sampled at a vertical resolution of 480 meters with 240 m oversampling averaged over a 1.4 km by 1.7 km footprint  
45 (cross and along track). The reflectivity profiles in Sc provided information on cloud structure and drizzle particle size (Kollias et al., 2011a, b). Since the launch in 2006, CS-CPR in synergy with other active and passive sensors in the NASA A-train constellation served as a key benchmark for climate models (e.g., Stephens et al., 2010), but also advanced a diversity of scientific understanding from aerosol-cloud interactions to warm rain formations (Leon et al., 2008; Takahashi et al., 2017; Suzuki et al., 2010; among many others). Despite the achievements and efforts, stratocumulus clouds are  
50 inherently challenging for spaceborne CPRs, given they are typically capped by a strong inversion with cloud thickness  $< 500$  m (e.g., Yang et al., 2018) and 50% of the sub-cloud rain echoes can be below 0.75 km (Lamer et al., 2020). For instance, 30-70% of cloudy columns in marine boundary layer clouds can be missed by CS-CPR due to the ground clutter (0.75~1 km), limited sensitivity, and coarse sampling range (Rapp et al., 2013; Christensen et al., 2013; Liu et al., 2018; Lamer et al., 2020).

55

With the decommissioning of NASA's CloudSat and CALIPSO satellites in 2023, the launch of EarthCARE satellite could therefore not come at a more opportune time. The Earth Clouds, Aerosol and Radiation Explorer (EarthCARE, Wehr et al., 2023) is a joint European/Japanese mission that was successfully launched in May 2024. The payload is composed of a 94-GHz Doppler Cloud Profiling Radar (EC-CPR hereafter), a high-spectral-resolution ATmospheric LIDar (ATLID), a multi-  
60 spectral imager (MSI) and a broadband radiometer (BBR). The composition resembles A-train in a way permitting synergistic approaches that integrate profiling capabilities of radar and lidar with the passive imagers providing broad cloud context.

65 EC-CPR is the first spaceborne cloud radar with Doppler capabilities, which open the opportunities of estimating vertical air motions and sedimentation rates on a global scale (Kollias et al., 2014). In addition, EC-CPR has improvements in several aspects regarding reflectivity measurements, compared to its predecessor CS-CPR. EC-CPR possesses a larger antenna (2.5 vs. 1.8 m diameter) and flies at lower altitude (~393 km vs. 705-732 km of CS-CPR), which allows an enhancement of sensitivity and a reduction of footprint size. The minimum detectable signal (MDS) of EC-CPR is around -35 dBZ, whereas CloudSat's MDS varied over the course of the mission being close to -30 dBZ in 2007 and ending near -25 dBZ in 2020 (personal communication, Roger Marchand). EC-CPR's instantaneous footprint at the surface level is 750 m (Wehr et al., 2023), approximately a factor of 2.3 (along track) and 4 (field-of-view area) smaller than the CS-CPR footprint. As such, the non-uniform beam filling (NUBF) effect is expected to be largely mitigated (Battaglia et al., 2021; Xu et al., 2025). In terms of vertical sampling, EC-CPR provides a finer range sampling at 100 m relative to CS-CPR at 240 m. Horizontally, along-track integration length is reduced to 500 m (Kollias et al., 2023) from 1.1 km of CS-CPR.

75 Drizzle detection with radar observations is an ongoing topic of interest. A threshold of radar reflectivity, typically ranging from -20 to -15 dBZ, is used to distinguish drizzling and non-drizzling clouds in many studies (Chin et al, 2000; Mace and Sassen, 2000; Kato et al., 2001; Wang and Geerts, 2003; Kogan et al., 2005; Leon et al., 2008; Lebsock et al., 2008; among others). In the CloudSat 2C-PRECIP-COLUMN product (Haynes et al., 2009), rain is flagged possible when near-surface reflectivity exceeds -15 dBZ with rain occurrence more certain with enhanced reflectivity. This threshold reflectivity can vary with cloud droplet number concentration and effective radius as well as liquid water path (LWP, Liu et al., 2008; Leon et al., 2008). Fewer studies explored the slope of CS-CPR reflectivity profiles in order to determine the onset of warm rain (Wang et al., 2017), which is based on where the maximum columnar reflectivity ( $Z_{max}$ ) is located in the vertical profile. The different locations of  $Z_{max}$  ( $H_{max}$ ) signal the different predominant microphysical processes. Reflectivity increases with height ( $Z_{max}$  closer to cloud top) within the non-raining clouds due to condensational growth. As the collision and coalescence processes becoming more efficient with drizzle development,  $Z_{max}$  is expected to move towards cloud base.

The primary objectives of this study are as follows:

- Evaluate the overall performance of the first-year EC-CPR observations regarding the detection of cloud and precipitation within Sc over the Southeast Pacific (SEP) and Southeast Atlantic (SEA) Ocean.
- Compare the existing EC-CPR observations of subtropical Sc with the climatology based on CS-CPR to understand the novel insights EC-CPR can introduce with its enhanced capabilities. A continuous long-term observational record of marine low clouds can be possible with consistency established and discrepancies well understood.
- Combining observations with a drizzle model, we investigate how the key information contained in reflectivity profiles regarding drizzle occurrence can be distorted by the radar point target response (PTR) and surface clutter.

## 2 Data and methodology

### 2.1 EarthCARE and CloudSat observations

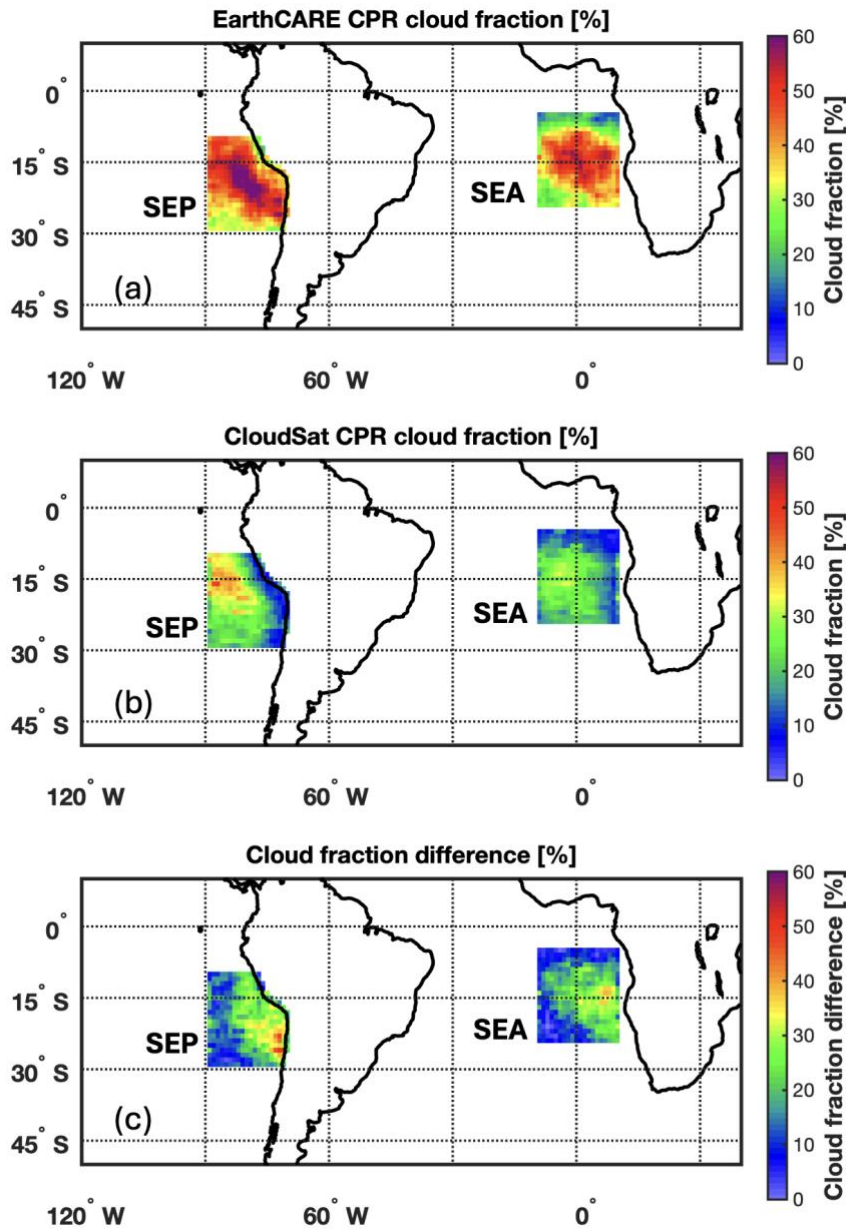
100 The EC-CPR observations cover the period from June 2024 to May19<sup>th</sup>, 2025 and include the radar reflectivity corrected for gaseous attenuation and the feature mask that identifies significant detections from hydrometeors and removes noise, ground-clutter and other artifacts (Kollias et al., 2023). Two years (2007 and 2008) of CS-CPR observations are used for comparison. The CS-CPR radar reflectivity and cloud mask are from the 2B-GEOPROF R05 (Marchand et al., 2008). The data analysis focuses on two 20×20° geographical regions that are well known for their strong climatology of low-level stratiform clouds. The first is in the Southeast Pacific (SEP), centered at 80° W and 20° S off the coast of Chile. The other is in the Southeast Atlantic (SEA), centered around 0° and 15° S off the coast of Angola and Namibia.

105

A number of criteria are applied to select single-layer marine low cloud profiles from the EC dataset: 1) “significant\_detection\_classification” is between 1 and 3, so as to exclude range bins that are identified to be contaminated by ground clutter with high confidence or other artifacts such as mirror images and multiple scattering tails. 2) continuous radar echo with reflectivity greater than -35 dBZ extend from below 1 km up to 3.5 km. An upper threshold from 3 to 4 km is often taken for Sc cloud regime as the majority of maritime Sc has cloud top below 3 km (Leon et al., 2008; Muhlbauer et al., 2014). 3) There are no measured reflectivities that exceed -35 dBZ within 1 km above the identified low-level clouds, so the identified layer clearly separated from higher clouds. 4) “land\_flag” is used to determine observations taken over the ocean surface. 5) At least two continuous cloudy range bins vertically are required.

115 Given the differences of radar system and data products, the criteria used for CloudSat are adjusted accordingly. 1) Consistent with previous studies (e.g., Muhlbauer et al., 2014), Cloud\_mask is  $\geq 20$  to remove clutter and very weak echoes with high uncertainty. 2) and 3) are the same as applied the in the EC data but use the minimum detectable signal of -30 dBZ as the threshold. 4) “Surface\_type” from 2C-Precip-COLUMN R05 (Haynes et al., 2009) is used to identify profiles over open ocean without sea ice. 5) applied to the EC dataset is not required for CloudSat, provided the different vertical resolution (240 vs. 100 m) and the shallow nature of Sc.

120



125 **Figure 1: (a) Spatial maps of cloud fraction from the first year of the EarthCARE CPR data for the studied regions over Southeast Atlantic (SEA) and Southeast Pacific (SEP) Ocean. (b) Same as in (a), but for the 2-year CloudSat CPR data from 2007 to 2008. Means of  $1 \times 1^\circ$  bins are shown. (c), the difference of cloud fraction between EarthCARE and CloudSat CPR. A 2D box smoothing is applied to reduce the noise in the spatial map, which does not affect the analysis in the remainder of the manuscript.**

Fig. 1 exhibits the spatial maps of mean cloud fraction for the studied regions, which are calculated by dividing the total number of identified Sc profiles by the total number of all observed profiles within  $1 \times 1^\circ$  bins. Cloud fraction estimated using EC-CPR (Fig. 1a) is on average 19% higher than the estimates based on CS-CPR (Fig. 1b). Despite the weak La Niña

130 forcing together with the abnormally warm SSTs in 2024-5 are inclined to cause modest decrease of Sc cloud fraction in the  
more offshore regions, EC-CPR detects overall higher cloud fraction due to its enhanced capability. The spatial  
characteristics of EC-CPR cloud fraction show good consistency with the climatology built upon 5 years of CS-CPR  
(Marchand et al., 2008) and CALIPSO (Mace et al., 2009) data (Fig. 2 in Muhlbauer et al., 2014), though about 20% more  
Sc clouds can only be detected with radar and lidar together. Moving westward and further offshore, cloud fraction is lower  
135 consistent with well-known tendency of the extensive Sc cloud decks in this region gradually breaking with cumulus  
developing under Sc, as boundary layer deepens, and stability reduces. The change of cloud features and mesoscale  
organizations is also reflected by the increased cloud top height (CTH) variability moving away from the coasts (Fig. S1 b  
and d). Near the coast Sc deck is capped by the strong inversion and frequently non- or lightly drizzling with low CTH,  
which is particularly challenging for spaceborne radars. EC-CPR shows an improvement as significant as ~30% in the  
140 detection of coastal Sc (Fig. 1c). In terms of radar-detected CTH, EC-CPR and CS-CPR diverge most near the coast (Fig. S1  
a and c). CTH is reported to be about 1–1.2 km just offshore of Chile/Peru and increase to 1.5–2 km by 85°W during the  
VOCALS Regional Experiment (Bretherton et al., 2010), which is quite consistent with the EC-CPR observations shown in  
Fig. S1a.

## 2.2 Drizzle model

145 A one-dimensional (1D) steady-state drizzle model is employed (Kollias et al., 2011) to help with the interpretation of the  
vertical structure of stratocumulus as documented by the EC-CPR. The model was developed to study the evolution of the  
drizzle DSDs within and below warm stratiform clouds, allowing for various assumptions for key parameters and processes,  
such as cloud number concentration ( $N_d$ ), LWP amount, autoconversion schemes, initial drizzle DSDs, and the vertical  
distribution of the cloud liquid water content (LWC) and the degree of adiabaticity. The vertical resolution of the model is 10  
150 m.

Cloud LWC increases with height above cloud base, the rate of which is determined by  $\Gamma_{ad}$  and  $f_{ad}$ .  $\Gamma_{ad}$  indicates the  
theoretically predicted growth rate in an adiabatic rising parcel. A constant value of  $\Gamma_{ad} = 1.8 \times 10^{-6} \text{ kg m}^{-4}$  is used here.  $f_{ad}$   
is the adiabaticity factor that represents the degree of departure from the adiabatic assumption due to mixing.  $f_{ad}$  is set to be  
155 either 1 (adiabatic) or follow the parameterization in Wood et al. (2009) where  $f_{ad}$  scales with height in the cloud layer.  
Cloud DSD is assumed to be lognormal.  $N_d$  is constant in the cloud layer, with the value specified to be 50, 100, 200, 400,  
750, or 1000  $\text{cm}^{-3}$ , representing a range of environments from pristine to very polluted. Cloud LWP is varied from about 50  
to 250  $\text{gm}^{-2}$ , which is consistent with the climatology of observed Sc clouds. Five autoconversion schemes are considered.  
Three of them parameterizes autoconversion solely as a function of cloud mass content and number concentration (Tripoli  
160 and Cotton 1980; Khairoutdinov and Kogan 2000; Wood 2005), whereas Liu and Daum (2004) uses cloud droplet larger  
order moments and Seifert and Beheng (2001) uses drizzle water mixing ratio.

165 The initial size distribution of injected drizzle via autoconversion is assumed to be a two-shape parameter generalized  
gamma distribution. The explicit calculation of the further stochastic growth of each drizzle size via the cloud droplet  
accretion is done using collision efficiency from Vohl et al. (2007). Observational study suggests that the choice of accretion  
rate formulation results in less diversity in comparison to the choice of autoconversion scheme (Wood 2005). As such, we  
use 5 different autoconversion parameterizations with the accretion formulation unchanged. The diameter of embryo drizzle  
drops is set to be either 60 or 80  $\mu\text{m}$ . Below clouds in the sub-saturated environment drizzle drops are subject to evaporation  
process. A linear decrease at 0.36  $\text{km}^{-1}$  is imposed for relative humidity below cloud base based on EPIC observations  
170 (Comstock et al., 2004).

A total of over 1500 reflectivity profiles are generated by combining 5 different  $N_d$ , varying LWP, 2 assumptions of cloud  
LWC profile ( $f_{ad} = 1$  or scales with height in the cloud layer), 5 autoconversion schemes, and 2 options regarding embryo  
drizzle size (60 or 80  $\mu\text{m}$ ). Other assumptions in the 1D drizzle model are fixed for this study.

### 175 **2.3 EC-CPR Point Target Response**

The radar point target response (PTR) describes how a radar system responds to an idealized "point target" (a target so small  
compared to the radar backscattering volume that it can be treated as a single scattering point in space). The EC-CPR PRT  
depends on the pulse length and on the receiver specifics. Understanding the PTR is very important for the interpretation of  
radar reflectivity profiles from shallow cloud systems such as low-level stratiform marine clouds. The PTR can smooth the  
180 reflectivity profiles, causing a reduction of peak reflectivity and an extension of cloud boundaries determined by radar  
echoes (Burns et al., 2016, Lamer et al., 2020).

Considering the Earth's surface as a point target, the clear-sky reflectivity profiles measured in proximity to the surface can  
be used to estimate the PTR. A CFAD composed of over 8 million EC-CPR reflectivity collected under clear-sky conditions  
185 with wind speeds between 7.5 and 8.5 m/s (thus  $\sigma_o$  about 10 dB, Sasikumar et al, 2025) is shown in Fig. 2. The red line  
indicates the derived median. Reflectivity peaks around 35 dBZ at the surface and rapidly decreases to -35 dBZ at the  
altitude of 0.5 km. The variability of surface echoes is subject to gaseous attenuation, the movement of satellite altitude and  
surface conditions (Burns et al., 2016). The strength of surface return varies within a few dB under the selected wind  
condition.

190

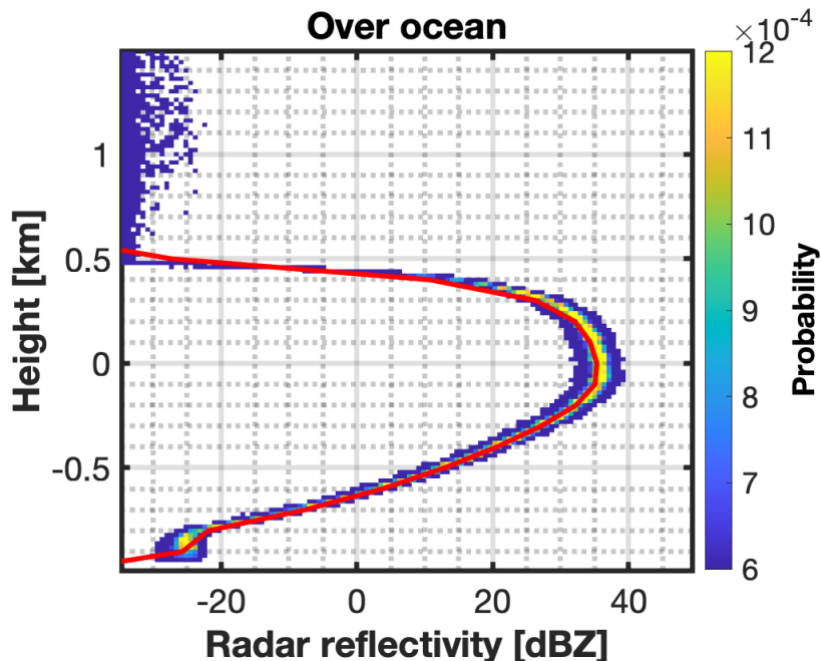
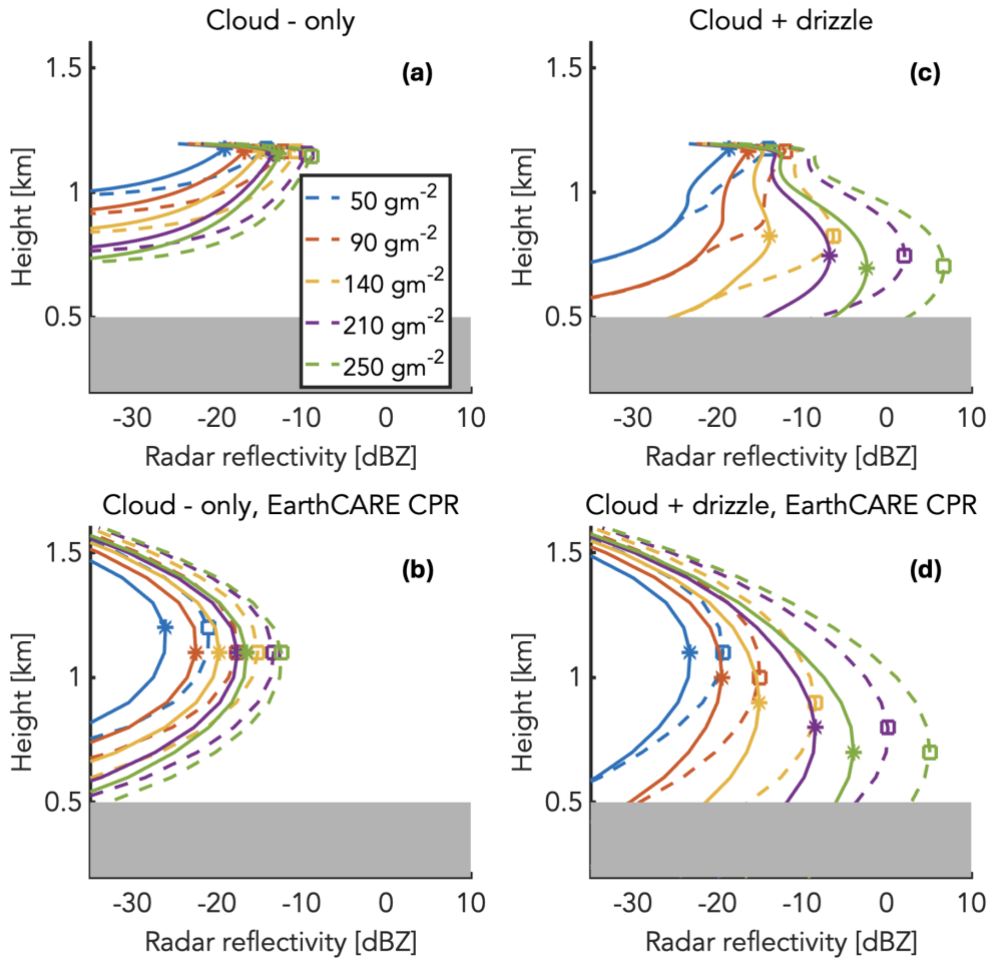


Fig. 2. Contour of Frequency by Altitude Diagram (CFAD) of over 8 million clear-sky reflectivity profiles observed by EC-CPR over ice-free ocean where wind speeds are within  $8 \pm 0.5$  m/s. The solid red line represents the derived median as the PTR function.

The EC-CPR PTR was designed to be asymmetric. The ground clutter is fully suppressed (below the EC-CPR MDS) 500 m above the sea surface while it has a gentler roll-off at negative heights (tail of the PTR). Therefore, it is different from the CS-CPR PTR that is largely symmetric (Lamer et al. 2020).

## 2.4 EC-CPR simulations

The 1D model “cloud only” and “cloud + drizzle” microphysical profiles are used as input to estimate the radar reflectivity at the model resolution (10 m) using T-matrix scattering. Figure 3a and c show ten radar reflectivity profiles for two different  $N_d$  values (50 and 200  $\text{cm}^{-3}$ ) and five LWP values between 51 to 252  $\text{gm}^{-2}$ . The top-row panels show the vertical profiles at model resolution and the bottom-row panels display what the EC-CPR would observe correspondingly. Prior to the application of the PTR, reflectivity tends to increase with height when there exist only cloud particles due to the condensational growth of the cloud droplets (Fig. 3a). The location of the maximum radar reflectivity ( $Z_{\text{MAX}}$ ) is indicated by squares and asterisks. In the cloud-only profiles,  $Z_{\text{MAX}}$  is close to the cloud top with values between -25 and -10 dBZ. In general, larger LWP leads to larger cloud reflectivity given the same  $N_d$ , and likewise smaller  $N_d$  results in larger cloud reflectivity provided the same LWP. For  $N_d$  this is due to the bigger droplets formed in the more pristine environment for the same LWP.



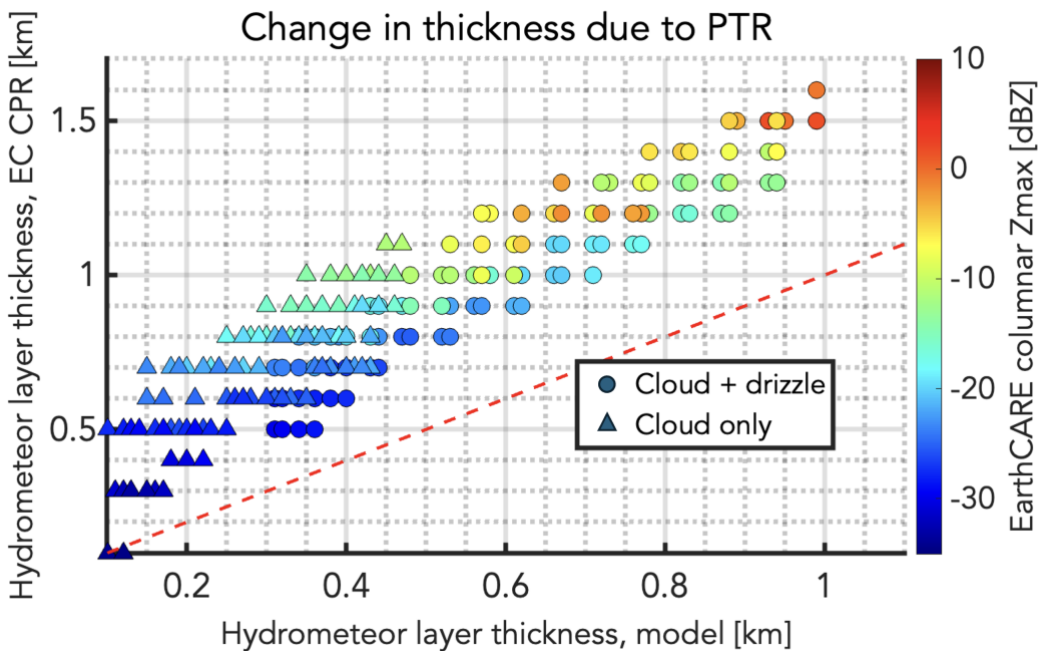
210 **Fig. 3. (a) Reflectivity profiles forward calculated from the 1D microphysical model output using the cloud only hydrometeors; (b) same as (a), but with the PTR applied. (c) Reflectivity profiles forward calculated from the 1D microphysical model output using both the cloud and drizzle hydrometeors (which correspond to the actual radar signal); (d) same as in (c), but with PTR applied. Solid and dash lines indicate that total number of cloud droplets per unit of volume ( $200$  and  $50 \text{ m}^{-3}$ , respectively). Colors indicate different cloud LWP in  $\text{gm}^{-2}$  as shown in legend. Asterisks and squares respectively represent the height of the  $Z_{\text{MAX}}$ . The gray zone indicates the region contaminated by the surface clutter.**

215 When drizzle particles are added to the cloud-only profiles, the processes of autoconversion and accretion that transfer water mass from the cloud to the drizzle category also contribute to the determination of the radar reflectivity profile. In this case (Fig. 3c), the height of  $Z_{\text{MAX}}$  ( $H_{\text{MAX}}$ ) tends to be lowered and within closer proximity to cloud base, the specific location of which varies with microphysics (Fig. 3c). This is consistent with surface-based observations (Frisch et al., 1995; Kollias et al., 2004; Serpetzoglou et al., 2008). The reflectivity starts to decrease as drizzle drops fall below cloud base under the effect of evaporation process (Yang et al., 2018; Ghate and Cadeddu, 2021). The values of  $Z_{\text{MAX}}$  are also significantly increased due to the presence of larger drizzle drops with range between  $-20$  to  $+5$  dBZ. It is worth noting that  $Z_{\text{MAX}}$  is often located

220 below cloud base with the existence of drizzle (e.g., Comstock et al, 2004) and therefore  $H_{\text{MAX}}$  cannot be simply interpreted

as an equivalent to cloud base height. In addition,  $H_{MAX}$  is not necessarily where rain rates ( $\sim D^4$ ) or total water mass ( $\sim D^3$ ) reaches the maximum due to the fact that reflectivity ( $\sim D^6$ ) is disproportionately sensitive to the larger drops in the volume. There is considerable overlap in the range of  $Z_{MAX}$  values in “cloud only” and “cloud + drizzle” profiles. Nevertheless, location of the  $Z_{MAX}$  ( $H_{MAX}$ ) and the morphology of the radar reflectivity profile could add critical information for the detection of drizzle particles in the radar reflectivity profiles of low-level stratiform clouds (Fig. 3a vs. c).

The forward simulated profiles of radar reflectivity for the cloud-only and cloud and drizzle profiles are convoluted in range with the EC-CPR PTR to simulate the vertical stretch effects of the 500 m pulse length using the methodology described in Lamer et al., 2020 (Fig. 3b, d). The EC-CPR PTR complicates the interpretation of the radar reflectivity profile. After applying the PTR, the shape of cloud-only reflectivity profiles (Fig. 3b) changes significantly and the initially asymmetrical profile becomes parabolic. The  $H_{MAX}$  shift lower, closer to the center of the CPR echo profile (Fig. 3b) instead of near the cloud top as shown in Fig. 3a. Also notable is the vertical stretching of cloud layers, with the top and bottom of the radar echo stretched upwards and downwards, respectively (Lamer et al., 2020). Thus, biases are introduced in terms of cloud boundaries based on radar signal returns (Burns et al., 2016). As for the drizzling scenario, the convolution with PTR smooths out the vertical change associated with microphysical processes and thickens the hydrometeor layer as well (Fig. 3d). More importantly, the PTR blurs the distinction between “cloud-only” and “cloud+drizzle” profiles that could have been made with the radar observations with high vertical resolution (short pulse) based on the relative position of  $Z_{MAX}$  in the vertical column.



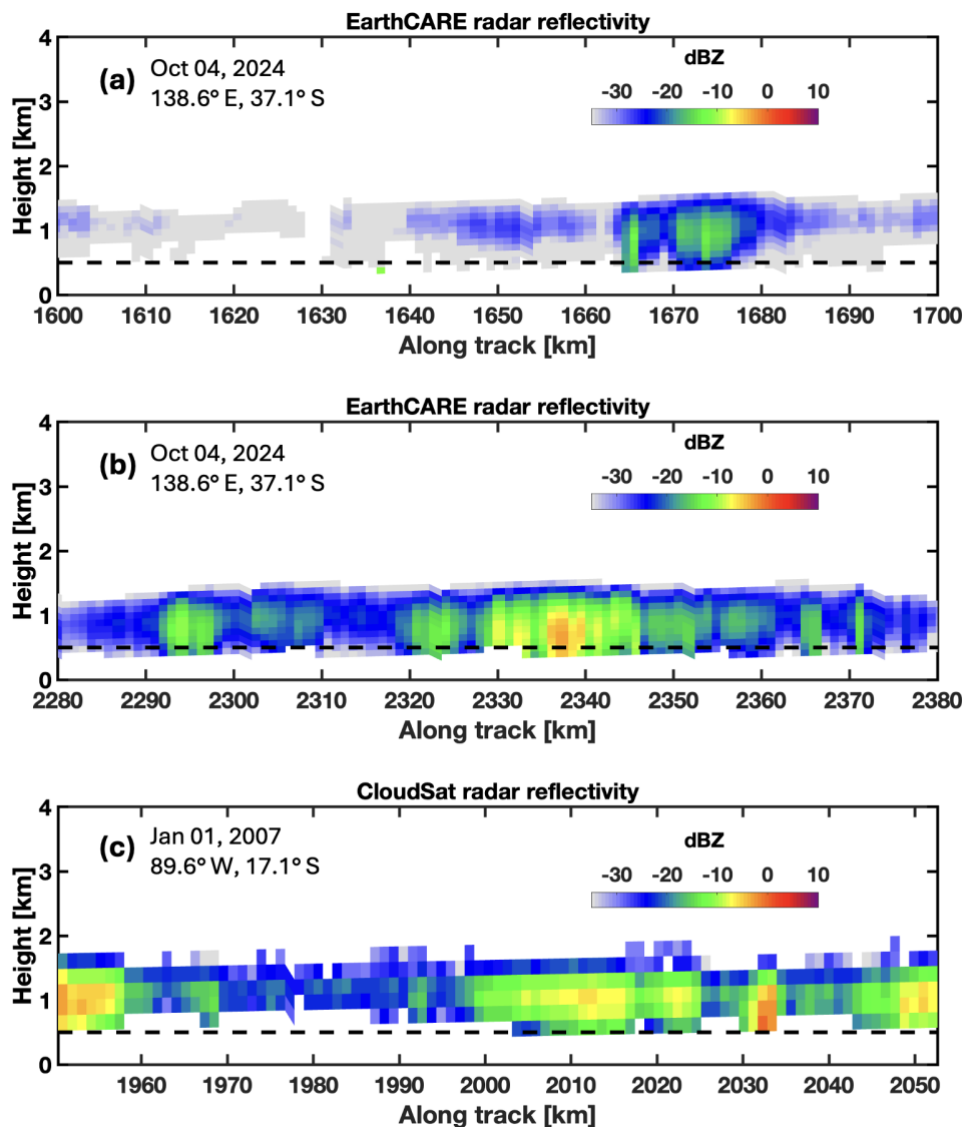
245 **Fig. 4. Model hydrometeor layer thickness with EC-CPR PTR convolved vs. model hydrometeor layer thickness without the PTR applied. Colors indicate the  $Z_{MAX}$  in the column. Circles represent “cloud+drizzle” profiles and triangles represent “cloud-only” profiles.**

250 The impact of the EC-CPR PTR on the observed thickness of low-level marine stratiform clouds is further demonstrated in Fig. 4. Using all the simulated EC-CPR reflectivity profiles of the 1D model output, the hydrometeor layer thickness ( $\Delta H$ ) with or without the PTR range convolutions applied and using the same minimum detectable signal as the EC-CPR is estimated. As expected, the application of the PTR shifts the relationship away from the 1:1 line. The  $\Delta H$  varies from 0.2 to 0.5 km in the cloud-only cases from the 1D model. After the convolution with PTR, most cloud-only  $\Delta H$  is between 0.4 and 1 km (triangles). The similar inflation of  $\Delta H$  is also observed in the “cloud+drizzle” cases with an average increase about 0.4-0.5 km (circles). As expected,  $\Delta H$  is overall thicker with the presence of drizzle. In addition, there appears to be a more significant change in  $\Delta H$  due to PTR for profiles with higher  $Z_{MAX}$ .

## 255 **3 Results**

### **3.1 Comparison with CloudSat and airborne radar observations**

260 The EarthCARE satellite was launched after the decommission of the CloudSat satellite, therefore no coincident measurements are available. Three 100-km along track observations of Sc from the EC-CPR (Fig. 5a and b) and CS-CPR (Fig. 5c) are presented to provide a quick overview of the qualitative differences between the two CPRs. Fig. 5a shows a tenuous thin Sc with  $Z_{MAX}$  often less than -28 dBZ. As a result, a large portion of the EC-CPR hydrometeor detection are expected to be missed by the CS-CPR due to their very weak radar echoes and their location below 1km. This suggests that the representativeness of cloud-only and lightly drizzling profiles is enhanced with the EC-CPR observations. Two additional EC-CPR and CS-CPR examples of thin non-precipitating low clouds with cloud top below 1 km are given in Fig. S2. CS-CPR more likely underdetects a larger part of a continuous cloud layer that is shallow and weakly reflective due to its  
265 limitations on sensitivity and surface clutter.

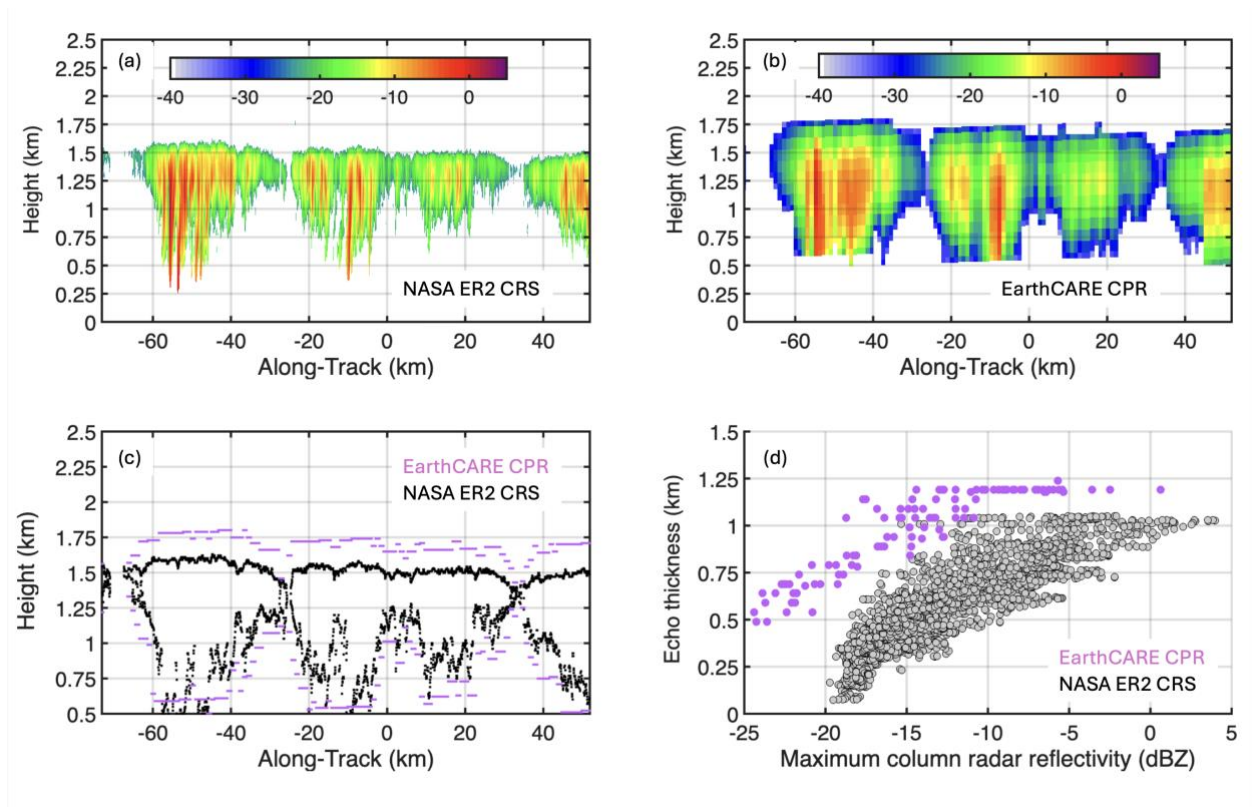


270 Fig. 5. (a) and (b), Two segments of marine low clouds observed by the EC-CPR on Oct 04, 2024, near 138.6° E and 37.1° S. Ground clutter is removed. (c), observations of CloudSat CPR (cloud mask  $\geq 20$ ) at 89.6° W and 17.1° S on Jan 01, 2007. Black dash lines indicate the height of 0.5 km.

The other two panels present similar drizzling scenarios that are detectable by both EC-CPR and CS-CPR. The cloud top of the EarthCARE case (Fig. 5b) appears lower and more flattened relative to the CloudSat case (Fig. 5c), which may be attributed to both the differences in PTR and the location and time of observations. In addition, a more complete profile can now be obtained with EC-CPR for clouds with reflectivity between about -25 and -15 dBZ that are subject to larger  
 275 uncertainties regarding drizzle occurrences. If we compare 2300-2320 m along track in Fig. 5b against 1970-1990 m along

track in Fig. 4c, the capability of EC-CPR to extend the detection to  $\sim 500$  m in such clouds could improve our ability to determine if the stratiform layer precipitates.

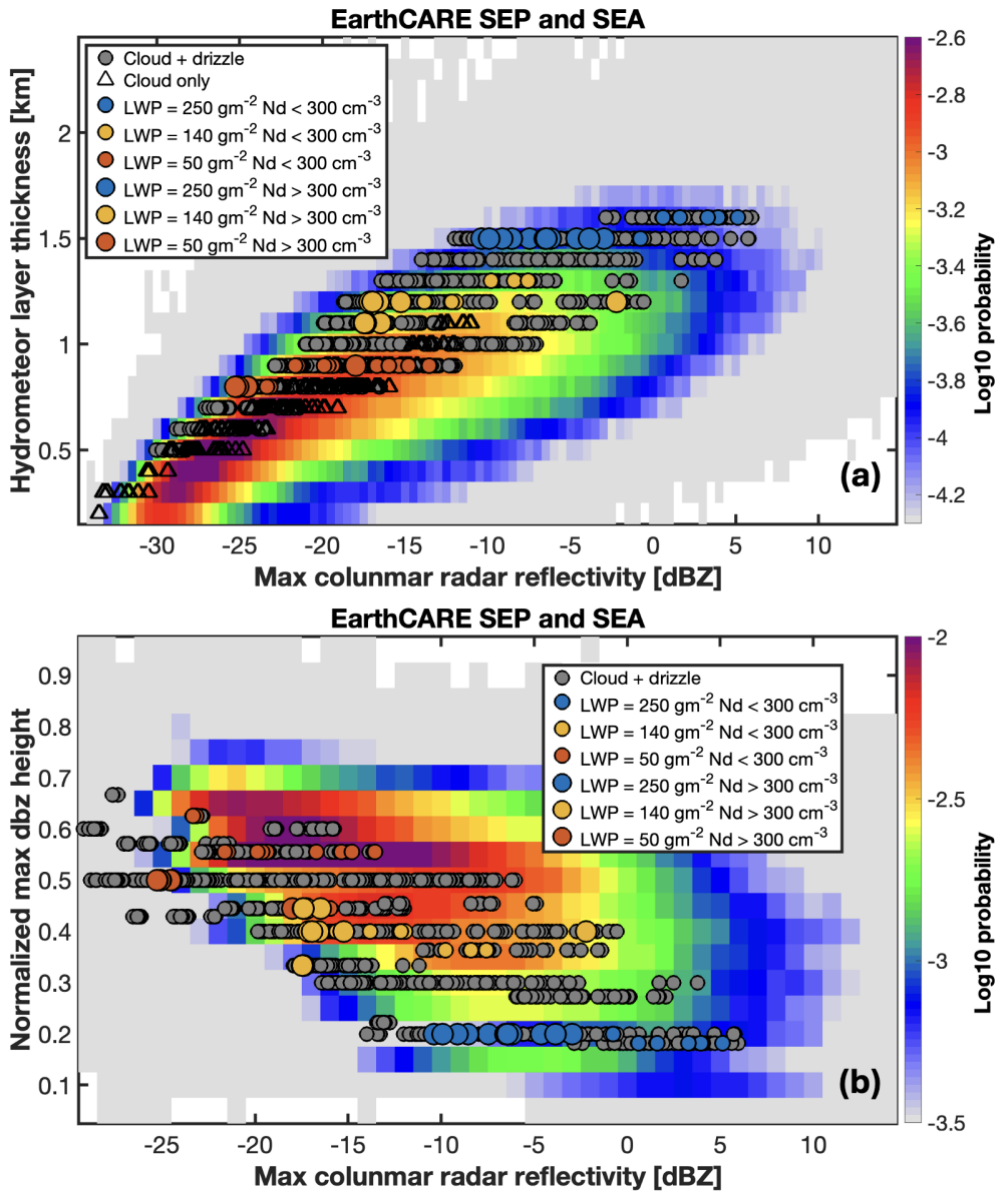
The Westcoast & Heartland Hyperspectral Microwave Sensor Intensive Experiment (WHyMSIE) took place in October and November 2024, which included coordinated underflights of EarthCARE for validation purposes. On Oct 30<sup>th</sup>, 2024, a marine stratiform cloud layer was observed off the coast of California by the EC-CPR and the Cloud Radar System (CRS, McLinden et al., 2021) on-board the NASA ER-2 high-altitude aircraft (Fig. 6). The RMS of ground track match was 429 meters, and the relative time was -7 to 5 minutes. The CRS is a 94-GHz cloud radar with a sensitivity of -30 dBZ at 10 km range and 0.5 s integration. Considering the ER-2 flying altitude (approximately 20 km) the effective sensitivity of the CRS is -25 dBZ at the altitude of the marine stratocumulus clouds. The vertical resolution is 115 m, which is approximately 5 times higher than that of the EC-CPR. The CRS along track resolution is 125 m which is 8 times finer than that of the EC-CPR.



290 Fig. 6. EarthCARE CPR and collocated NASA ER-2 CRS observations of marine stratus collected on Oct 30<sup>th</sup>, 2024, near 121.7° W and 26.6° N. (a) radar reflectivity [dBZ] measured by ER-2 CRS and (b) EarthCARE CPR, respectively. (c) cloud top and base height determined with radar reflectivity from the EarthCARE CPR (purple) and ER2 CRS (black). (d) Hydrometeor layer thickness based on radar echoes vs. the maximum columnar radar reflectivity.

The agreement between the EC-CPR and CRS observations is very encouraging (Fig. 6). The EC-CPR captures most of the cloud and precipitation features despite the horizontal and vertical smoothing and stretching induced by the PTR and the CPR footprint (~800 m). The cloud top determined by the EC-CPR is about 150-200 m taller than that of the CRS (Fig. 6a, b and c). This is consistent with the analysis of the modelled radar reflectivity profiles. The ground clutter is within close proximity to 500 m as predicted by the PTR. Also noticeable is the thickening of the clouds due to the EC-CPR PTR that stretches clouds both upwards and downwards (Fig. 6c). Evident in both ER2 and EarthCARE observations, there is a similar positive correlation between  $Z_{MAX}$  and the hydrometeor layer thickness determined by radar (Fig. 6d).

Ambiguities exist when it comes to partition cloud and drizzle with single-frequency radar reflectivities (e.g., Xu et al., 2019). The variability associated with microphysics, dynamics and the fact that reflectivity is dominated by the large drops in the radar volume all contribute. Therefore, using a threshold of  $Z_{MAX}$  for drizzle detection is subject to uncertainties. Combining the model outputs and the EC-CPR reflectivity profiles allows for some exploration of the possibility to identify a multi-variable relationship beyond a simple threshold of reflectivity. For that purpose, the joint probability distribution between observed hydrometeor layer thickness ( $\Delta H$ ) and  $Z_{MAX}$  in low-level marine stratiform clouds in the EC-CPR observation is examined next (Fig. 7a). As expected, the maximum EC-CPR reflectivity in the column ( $Z_{MAX}$ ) increases as  $\Delta H$  increases. The overlaid model data are after the convolution with the PTR and with the existence of ground clutter (~0.5 km) considered. Within the full spectrum of  $\Delta H$ , it is almost certain drizzle-free (black triangles) at the lower end and drizzle-present (circles) at the higher end. The differentiation of “cloud-only” and “cloud+drizzle” with radar alone seems most challenging in the domain where  $\Delta H$  is 0.7~1km and  $Z_{MAX}$  ranges from -25 to -15 dBZ. The positive correlations between  $\Delta H$  and  $Z_{MAX}$  shown in Fig. 7a is evident in both the EC-CPR observations and the forward simulated model output. Nature carries more variability, and the employed 1D steady model can only capture the frequently observed events. Thicker clouds and larger  $Z_{MAX}$  imply an enhanced amount of LWP (indicated by filled circles). The constraints of these observables on cloud  $N_d$  are more complicated with a tendency of  $N_d$  negatively correlated with  $Z_{MAX}$ . The nonlinear relationships are also present in the covariance of  $Z_{MAX}$  with LWP and cloud effective radius that are investigated by Leon et al. (2008).



320 Fig. 7. (a) Probability distributions of Sc cloud thickness vs. the maximum radar reflectivity in the column observed by EC-CPR  
 325 from June 2024 to May 2025 in SEP and SEA. Triangles indicate “cloud-only” model runs convolved with EC PTR. Purple circles  
 indicate all the “cloud+drizzle” model runs convolved with EC PTR. Circles with filled colors in different size highlight subsets of  
 model runs with different LWP and Nd as indicated in the legend. (b) Probability distributions of Sc normalized height of Z<sub>MAX</sub> vs.  
 the maximum radar reflectivity in the column observed by EC-CPR. Profiles with hydrometeor layer thickness smaller than 0.7  
 km are excluded so as to mainly focus on the “cloud+drizzle” scenario. Profiles with Z<sub>MAX</sub> just above the ground clutter are not  
 included. Overlaid circles are the same as in panel (a).

Finally, we examine the relationship between the normalized height of  $Z_{MAX}$  ( $NH_{MAX}$ ) and  $Z_{MAX}$  (Fig. 7b).  $NH_{MAX}$  is defined as  $(H_{MAX} - H_{CB})/\Delta H$ , where  $H_{MAX}$  is the height of the  $Z_{MAX}$ ,  $H_{CB}$  is the observed hydrometeor base height and  $\Delta H$  is the observed hydrometeor layer thickness. Here cloud base and thickness are determined with radar echoes above MDS. Also, the EC-CPR profiles with  $Z_{MAX}$  found at the range bin just above the surface clutter are excluded, since the true  $Z_{MAX}$  might be within the clutter. The observed  $NH_{MAX}$  of cloud-only and light drizzling profiles is close to 0.5. We know from ground-based and airborne radar observations (Kollias et al., 2011; Remillard et al., 2013; Fan et al., 2018) that the  $NH_{MAX}$  of cloud-only and light drizzling profiles is usually near the cloud top. Thus, the PTR limits our ability to diagnose the absence of drizzle particles using the  $NH_{MAX}$  value. As the size and number concentration of drizzle particles in the profile increases,  $Z_{MAX}$  increases and  $NH_{MAX}$  decreases but the PRT has reduced the dynamic range of the  $NH_{MAX}$  compared to those from the model simulations without the PRT (Fig. 3). Further effort would be devoted to combining other observations that could afford additional constraints on drizzle detection such as Doppler velocity and path integrated attenuation (PIA).

### 3.2 Statistical comparison EC- and CS-CPR observations in marine stratus clouds

One way to evaluate the overall performance of EC-CPR against that of the CS-CPR in the detection of low-level stratiform marine clouds is to rely on statistics collected over a large spatial domain (the two marine stratocumulus basins (SEP and SEA) shown in Fig.1) and over a large temporal window (1 year for EC, 2 years for CloudSat). The reflectivity-height histogram of CPR echoes from the EC and CS are shown in Fig. 8a and b, respectively. Sc clouds are selected based upon the criteria as introduced in Section 2. The impact of the higher sensitivity and improved suppression of the surface echo are clearly visible. The two spaceborne CPR have radar echoes concentrated below 1.5 km and similar detections when reflectivity is  $> -12$  dBZ. CS-CPR appears to have a better signal to clutter ratio at low altitudes at high reflectivity and therefore more capable in terms of observing heavy snowfall (Coppola et al., 2025). Nevertheless, the EC-CPR detect significantly more echoes in the lowest km below  $-20$  dBZ, due to its higher sensitivity and improved surface clutter suppression. It is evident that the EC-CPR has enhanced capabilities to observe Sc clouds with weak echoes and possibly virga. The Sc cloud fraction (fraction of columns with a detection) as observed by EC-CPR and CS-CPR is approximately 40% (44.8% in SEP and 36.7% in SEA) and 20% (23.6% in SEP and 19.2% in SEA), respectively.

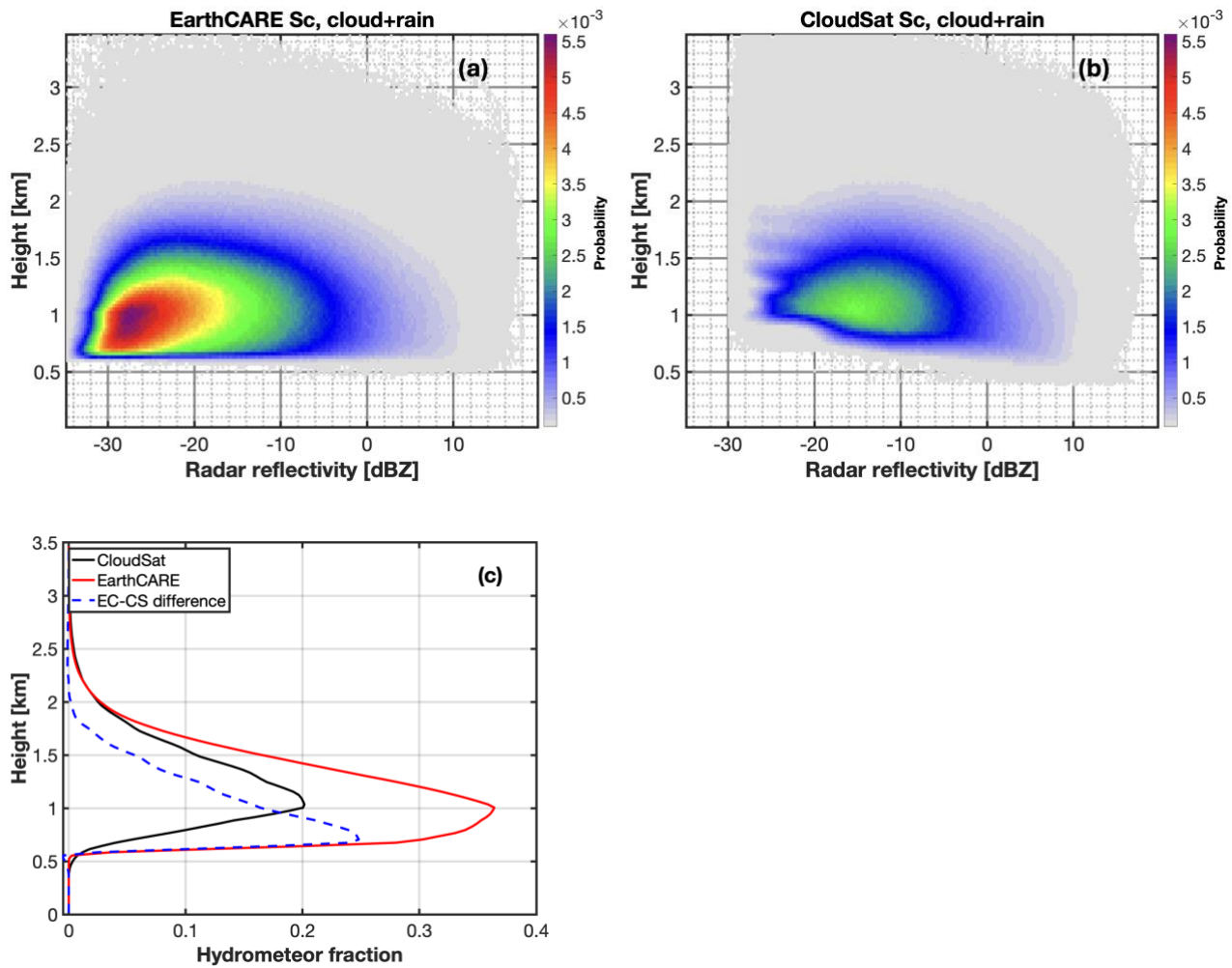


Fig. 8. (a) Reflectivity-height histogram of stratocumulus observed by the EarthCARE CPR from June 2024 to May 19<sup>th</sup>, 2025, off South America and Africa coasts; (b) Same as in (a), but for CloudSat CPR observations from 2007 to 2008. The vertical bin spacing is 30 m. The same interpolation to the 30-m bins is applied to both datasets. (c) Vertical profile of the hydrometeor detection fraction from each sensor and the difference (blue dash line) between EarthCARE and CloudSat.

355  
 360 The maximum radar reflectivity in the column ( $Z_{MAX}$ ) is frequently used to determine the presence of drizzle in low-level stratiform clouds (Frisch et al., 1995; Liu et al., 2008; Kollias et al., 2011a). In CloudSat, if the  $Z_{MAX}$  is higher than -15 dBZ, the profile was considered as containing drizzle (Lebsock et al., 2008). Here, the same definition for the detection of drizzle in the profile will be used in the EC-CPR observations. We will focus on the impact of the improved features of the EC-CPR in the determination of the fraction of drizzling profiles. In particular, since the EC-CPR extends the detection capability  
 365 down to 0.5 km above the ground, we will use the EC-CPR observations as a benchmark to quantify the misdetections by the CS-CPR due to its higher blind zone.

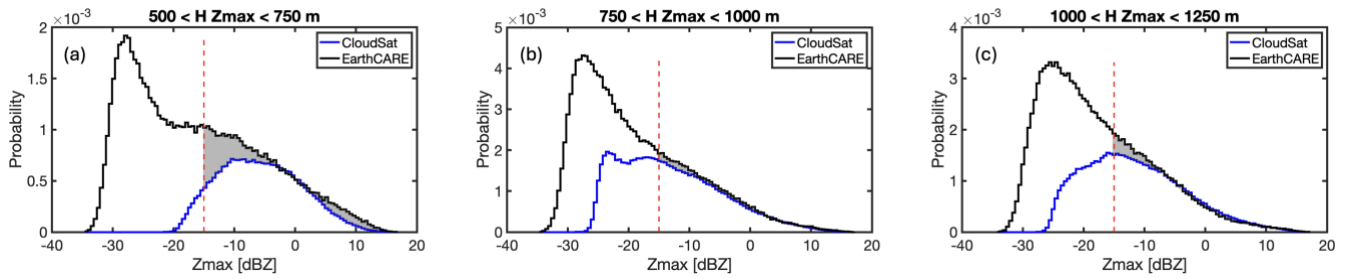


Fig. 9. The probability distribution  $Z_{MAX}$  values at different height ranges above the ocean surface: (a) between 500 and 750 m; (b) between 750 and 1000 m; and (c) between 1000 and 1250 m. Black and blue lines respectively indicate the EC-CPR and CS-CPR observations collected in SEA and SEP. The three categories are responsible for a Sc cloud fraction of 7.5%, 14.7%, 12.4% for EC and 2.7%, 7.9%, 6.4% for CloudSat, respectively. The red dash lines mark where  $Z_{MAX}$  is -15 dBZ; precipitating Sc are identified to correspond to the region located to the right of such lines. The three categories are responsible for a precipitating Sc cloud fraction of 3%, 4.4%, 4% for EC and 2.4%, 4%, 3.8% for CloudSat, respectively. The areas shaded in gray highlight the difference where  $Z_{MAX}$  is greater than -15 dBZ.

370

375

The probability distributions of  $Z_{MAX}$  from nearly one year of EarthCARE and two years of CloudSat observations in the two marine stratocumulus basins (SEP and SEA) are shown in Fig. 9. The  $Z_{MAX}$  dataset is conditionally sampled based on the height where the  $Z_{MAX}$  is observed. The probability is calculated by scaling the counts of each bin on the x axis by the total number of cloudy and clear-sky profiles of CloudSat and EarthCARE datasets, respectively.

380

The distribution of  $Z_{MAX}$  observed by EC-CPR is clearly more skewed to lower reflectivity in comparison with CS-CPR. The enhanced MDS significantly improves the detection of cloud-only and weakly drizzling components. The bimodality of CS-CPR  $Z_{MAX}$  reported but unexpected by Leon et al. (2008) is also noticeable here for the subset with  $H\_Zmax$  ranging from 750 and 1000 m (blue line in Fig. 9b), though a single mode of  $Z_{MAX}$  exists in the other subsets. We found that the mode with CS-CPR reflectivity smaller than -20 dBZ in Fig. 9b is mainly composed of profiles that have only one radar range bin above MDS. The bimodality could be due to the coarse vertical sampling of CS-CPR or an enhancement of reflectivity due to noise. The fraction of precipitating Sc observed by EC-CPR and CS-CPR is respectively 11.4% and 10.2%, summing the three height categories in Fig. 9. Overall CS-CPR misses the precipitation detection in Sc clouds by about 10.5%. As the height window of  $Z_{MAX}$  decreases,  $Z_{MAX}$  needs to be higher to be accurately detected by the CS-CPR. Considering -15 dBZ as the threshold to determine rain occurrence, CS-CPR misses increasing amount of raining profiles as  $H\_Zmax$  reduces. The missed detections are the largest if  $H_{MAX}$  is lower than 750 m (Fig. 9a), with about 20% of the raining profiles that are captured by EC-CPR are not detected by CS-CPR.

390

395

When  $H\_Zmax$  is > 750 m, one would expect that two sensors have the same level of skills in terms of detecting drizzle, while EC-CPR observed slightly more drizzle (Fig. 9 b and c). A factor that contributes these differences is that the sampling periods are different in this comparison, since CS-CPR and EC-CPR do not have coincident observations. The slightly

weaker inversions and warmer than average SSTs in 2024-5 tend to favor deeper boundary layer and more mixed stratocumulus-cumulus clouds that carry larger liquid water path with higher chance to rain, whereas the colder SSTs combined with strong inversions in 2007-8 favor overcast Sc with overall less precipitation.

#### 400 **4 Summary**

The Cloud Profiling Radar (CPR) onboard the EarthCARE satellite mission provides enhanced measurement capabilities relative to its predecessor, the CloudSat CPR. Operating at the similar frequency and pulse length, the EarthCARE CPR (EC-CPR) offers finer spatial sampling, an approximately +7 dBZ improvement in sensitivity, and substantially reduced surface clutter contamination. These advancements are particularly beneficial for the detection and characterization of  
405 marine stratocumulus (Sc) clouds.

In this study, we assess the overall performance of EC-CPR using the first-year (2024-5) observations collected over two  $20^\circ \times 20^\circ$  domains in the Southeast Pacific and Southeast Atlantic Oceans, regions known for persistent stratocumulus clouds. EC-CPR data are evaluated against coincident and collocated aircraft radar measurements and compared with CloudSat-  
410 based climatology from 2007-8 when the sensitivity of CS-CPR at its best, since EarthCARE was launched after the decommission of CloudSat. In addition, we investigate how the point target response (PTR) influences EC-CPR reflectivity profiles and drizzle identification. Using a drizzle microphysics model that generates “cloud-only” and “cloud + drizzle” profiles, combined with a radar simulator that forward calculates radar observables, we quantify how PTR-induced distortions affect reflectivity profiles and the interpretation of drizzle in stratocumulus systems.

415

The EC-CPR observations confirm that surface clutter contamination is effectively suppressed below 0.5 km due to the asymmetric shape of the PTR. As a result, hydrometeor detection is possible approximately 0.25–0.5 km closer to the surface compared to the CS-CPR.

420 For the marine stratocumulus (Sc) regions analysed in this study, CS-CPR estimates an average cloud fraction of about 20% (Fig. 1), whereas EC-CPR yields an average of approximately 40%, nearly double, despite the weak La Niña forcing together with the warmer than average SSTs in 2024-5 tend to cause modest decrease of Sc cloud fraction in the more offshore regions. This value, however, remains about 20% lower than the estimate obtained using a synergistic combination of CS-CPR and CALIPSO (Fig. 2 in Mülhbauer et al., 2014). The geographical distribution of cloud fraction derived from  
425 EC-CPR alone agrees well with previous results based on CS-CPR and CALIPSO, successfully capturing the observed transition from overcast stratocumulus to broken cumulus regimes moving westward and offshore. In addition, EC-CPR shows significant improvement in detecting coastal Sc decks that are weakly reflective with low cloud top height.

430 Compared with CS-CPR, EC-CPR demonstrates a clear advantage in detecting non-drizzling and weakly drizzling stratocumulus. The fraction of cloudy profiles below 1 km with reflectivities weaker than  $-20$  dBZ is substantially underestimated by CS-CPR. When a column-maximum reflectivity threshold of  $Z_{MAX} > -15$  dBZ is used to identify raining profiles, CS-CPR underestimates rainfall occurrence by up to 20% when  $Z_{MAX}$  occurs between 500 and 750 m. This underestimation diminishes when  $Z_{MAX}$  is either larger or located higher in the cloud column. Overall CS-CPR misses the precipitation detection in Sc clouds by about 10.5% for  $Z_{MAX}$  located between 500 and 1250 m.

435

EC-CPR reflectivity measurements closely replicate coincident airborne radar observations, though, as expected, cloud layers appear thicker at the coarser EC-CPR resolution. The influence of the PTR stretches clouds both upward and downward, resulting in an average overestimation of cloud thickness by 0.4–0.5 km in drizzling conditions. This degree of vertical stretching correlates positively with  $Z_{MAX}$  and the true cloud depth (Fig. 6).

440

The PTR also induces a parabolic shaping of reflectivity profiles relative to the modeled truth, affecting both non-drizzling and drizzling clouds. Consequently, the distinct contrast between the top-heavy profiles typical of non-drizzling clouds and the bottom-heavy profiles characteristic of drizzling clouds is reduced. Given the magnitude of this effect and the  $Z_{MAX}$  does not necessarily maximize where the precipitation is most abundant, additional observational constraints—beyond  $Z_{MAX}$  and  $H_{Z_{MAX}}$  should be explored, such as Doppler velocity and path-integrated attenuation (PIA).

445

Finally,  $Z_{MAX}$  tends to scale with cloud thickness, a relationship evident in both EC-CPR observations and the drizzle model simulations. The model also reveals an overall increase in liquid water path (LWP) with  $Z_{MAX}$  and cloud thickness, although the relationship between droplet number concentration (Nd) and reflectivity is more complex and requires further investigation.

450

455

### **Code/data availability**

EarthCARE data are publicly available from the ESA portal, <https://earth.esa.int/eogateway/missions/earthcare/data>. CloudSat 2B-GEOPROF(R05) is available at <https://www.cloudsat.cira.colostate.edu/data-products/2b-geoprof>. The

460 EarthCARE CPR point target response function is available in the Supplement. Code and the 1D model data are available upon request.

### **Author contributions**

ZX performed the analysis, generated the figures, and drafted the manuscript. PK provided the supervision and reviewed the manuscript. SS conducted the analysis of the CloudSat CPR data. AB provided the feedback on the results and the  
465 manuscript. BPT and MWM provided the EarthCARE CPR and ER-2 CRS data, respectively.

### **Competing interests**

The authors declare that they have no conflict of interest.

### **Acknowledgements**

PK was supported by the European Space Agency (ESA) under the EarthCARE Data Innovation and Science Cluster (DISC)  
470 project (AO/1-12009/24/I-NS). PK and ZX were also supported by the National Aeronautics and Space Administration (NASA) under the Atmospheric Observing System (AOS) project (Contract number: 80NSSC23M0113).

### **References**

- Battaglia, A., Kollias, P., Dhillon, R., Lamer, K., Khairoutdinov, M., and Watters, D.: Mind the gap – Part 2: Improving quantitative estimates of cloud and rain water path in oceanic warm rain using spaceborne radars, *Atmos. Meas. Tech.*, 13,  
475 4865–4883, <https://doi.org/10.5194/amt-13-4865-2020>, 2020.
- Bretherton, C. S., Wood, R., George, R. C., Leon, D., Allen, G., and Zheng, X.: Southeast Pacific stratocumulus clouds, precipitation and boundary layer structure sampled along 20° S during VOCALS-REx, *Atmos. Chem. Phys.*, 10, 10639–10654, <https://doi.org/10.5194/acp-10-10639-2010>, 2010.
- Burns, D., Kollias, P., Tatarevic, A., Battaglia, A., and Tanelli S.: The performance of the EarthCARE Cloud Profiling Radar  
480 in marine stratiform clouds, *J. Geophys. Res. Atmos.*, 121, 14, 525–14,537, doi:10.1002/2016JD025090, 2016.
- Chin, H., et al.: A microphysical retrieval scheme for continental low-level stratiform clouds: Impacts of the subadiabatic character on microphysical properties and radiation budgets, *Mon. Weather Rev.*, 128, 2511 – 2527, 2000.
- Christensen, M. W., Stephens, G. L., and Lebsock, M. D.: Exposing biases in retrieved low cloud properties from CloudSat: A guide for evaluating observations and climate data, *J. Geophys. Res.-Atmos.*, 118, 12120–  
485 12131, <https://doi.org/10.1002/2013JD020224>, 2013.

- Comstock, K. K., Wood, R., Yuter, S. E., and Bretherton, C. S., 2004: Reflectivity and rain rate in and below drizzling stratocumulus. *Q. J. R. Meteorol. Soc.*, **130**, 2891-2918.
- Coppola, M., Battaglia, A., Tridon, F., and Kollias, P.: Improved hydrometeor detection near the Earth's surface by a conically scanning spaceborne W-band radar, EGU sphere [preprint], <https://doi.org/10.5194/egusphere-2025-416>, 2025.
- 490 Eastman, R. I., McCoy, L., and Wood, R.: Environmental and internal controls on Lagrangian transitions from closed cell mesoscale cellular convection over subtropical oceans. *Journal of the Atmospheric Sciences*, **78**, 2367–2383. <https://doi.org/10.1175/JAS-D-20-0277.1>, 2021.
- Frisch, A. S., Fairall, C. W., and Snider, J. B.: Measurement of Stratus Cloud and Drizzle Parameters in ASTEX with a Ka-Band Doppler Radar and a Microwave Radiometer. *J. Atmos. Sci.*, **52**, 2788–2799, [https://doi.org/10.1175/1520-0469\(1995\)052<2788:MOSCAD>2.0.CO;2](https://doi.org/10.1175/1520-0469(1995)052<2788:MOSCAD>2.0.CO;2), 1995.
- 495 Gbate, V. P., and Cadet, M. P.: Drizzle and turbulence below closed cellular marine stratocumulus clouds. *Journal of Geophysical Research: Atmospheres*, **124**, 5724–5737. <https://doi.org/10.1029/2018JD030141>, 2019.
- Glienke, S., Kostinski, A., Fugal, J., Shaw, R., Borrmann, S., and Stith, J.: Cloud droplets to drizzle: Contribution of transition drops to microphysical and optical properties of marine stratocumulus clouds. *Geophysical Research Letters*, **44**, 8002–8010. <https://doi.org/10.1002/2017GL074430>, 2017.
- 500 Goren T., Rosenfeld D., Sourdeval O., and Quaas J.: Satellite Observations of Precipitating Marine Stratocumulus Show Greater Cloud Fraction for Decoupled Clouds in Comparison to Coupled Clouds. *Geophys Res Lett.* 2018 May 28;45(10):5126-5134. doi: 10.1029/2018GL078122, 2018.
- Hartmann, D. L., Ockert-Bell, M. E., and Michelsen, M. L.: The Effect of Cloud Type on Earth's Energy Balance: Global Anal- ysis, *J. Climate*, **5**, 1281–1304, [https://doi.org/10.1175/1520-0442\(1992\)005<1281:TEOCTO>2.0.CO;2](https://doi.org/10.1175/1520-0442(1992)005<1281:TEOCTO>2.0.CO;2), 1992.
- 505 Haynes, J. M., L'Ecuyer, T. S., Stephens, G. L., Miller, S. D., Mitrescu, C., Wood, N. B., and Tanelli, S.: Rainfall retrieval over the ocean with spaceborne W-band radar, *J. Geophys. Res.*, **114**, D00A22, doi:10.1029/2008JD009973, 2009.
- Kato, S., et al.: Doppler cloud radar derived drop size distributions in liquid water stratus clouds, *J. Atmos. Sci.*, **58**, 2895–2911, 2001.
- 510 King, M. D., Platnick, S., Menzel, W. P., Ackerman S. A., and Hubanks, P. A.: Spatial and Temporal Distribution of Clouds Observed by MODIS Onboard the Terra and Aqua Satellites, in *IEEE Transactions on Geoscience and Remote Sensing*, vol. 51, no. 7, pp. 3826-3852, July 2013, doi: 10.1109/TGRS.2012.2227333, 2013.
- Khairoutdinov, M., and Kogan, Y.: A new cloud physics parameterization in a large-eddy simulation model of marine stratocumulus. *Mon. Wea. Rev.*, **128**, 229-243, 2000.
- 515 Kogan, Z. N., Mechem, D. B., and Kogan Y. L.: Assessment of variability in continental low stratiform clouds based on observations of radar reflectivity, *J. Geophys. Res.*, **110**, D18205, doi:10.1029/2005JD006158, 2005.
- Kollias, P., Fairall, C. W., Zuidema, P., Tomlinson, J., and Wick, G. A.: Observations of marine stratocumulus in SE Pacific during the PACS 2003 cruise. *Geophys. Res. Lett.*, **31**, L22110, doi:10.1029/2004GL020751, 2004.
- Kollias, P., Rémillard, J., Luke, E., and Szyrmer, W.: Cloud radar Doppler spectra in drizzling stratiform clouds: 1. Forward

- 520 modeling and remote sensing applications, *J. Geophys. Res.*, 116, D13201, doi:[10.1029/2010JD015237](https://doi.org/10.1029/2010JD015237), 2011a.
- Kollias, P., Szyrmer, W., Rémillard, J., Luke, E.: Cloud radar Doppler spectra in drizzling stratiform clouds: 2. Observations and microphysical modeling of drizzle evolution, *J. Geophys. Res.*, 116, D13203, doi:[10.1029/2010JD015238](https://doi.org/10.1029/2010JD015238), 2011b.
- Kollias, P., Tanelli, S., Battaglia, A., and Tatarevic, A. Evaluation of EarthCARE Cloud Profiling Radar Doppler velocity measurements in particle sedimentation regimes, *J. Atmos. Oceanic Technol.*, 31(2), 366–386, doi:[10.1175/JTECH-D-11-00202.1](https://doi.org/10.1175/JTECH-D-11-00202.1), 2014.
- 525 Kollias, P., Puidgomènech Treserras, B., Battaglia, A., Borque, P. C., and Tatarevic, A.: Processing reflectivity and Doppler velocity from EarthCARE's cloud-profiling radar: the C-FMR, C-CD and C-APC products, *Atmos. Meas. Tech.*, 16, 1901–1914, <https://doi.org/10.5194/amt-16-1901-2023>, 2023.
- Lamer, K., Kollias, P., Battaglia, A., and Preval, S.: Mind the gap – Part 1: Accurately locating warm marine boundary layer clouds and precipitation using spaceborne radars, *Atmos. Meas. Tech.*, 13, 2363–2379, <https://doi.org/10.5194/amt-13-2363-2020>.
- 530 Lebsack, M. D., Stephens, G. L., and Kummerow C.: Multisensor satellite observations of aerosol effects on warm clouds, *J. Geophys. Res.*, 113, D15205, doi:[10.1029/2008JD009876](https://doi.org/10.1029/2008JD009876), 2008.
- L'Ecuyer, T. S., W. Berg, J. Haynes, M. Lebsack, and T. Takemura (2009), Global observations of aerosol impacts on precipitation occurrence in warm maritime clouds, *J. Geophys. Res.*, 114, D09211, doi:[10.1029/2008JD011273](https://doi.org/10.1029/2008JD011273).
- 535 Leon, D. C., Wang, Z., and Liu, D.: Climatology of drizzle in marine boundary layer clouds based on 1 year of data from CloudSat and Cloud-Aerosol Lidar and Infrared Pathfinder Satellite Observations (CALIPSO). *J. Geophys. Res.*, 113, D00A14, doi:[10.1029/2008JD009835](https://doi.org/10.1029/2008JD009835), 2008.
- Liu, Y. and Daum, P. H.: Parameterization of the autoconversion process. Part I: Analytical formulation of the Kessler-type parameterizations., *J. Atmos. Sci.*, **61**, 1539-1548, 2004.
- 540 Liu, Y., Geerts, B., Miller, M., Daum, P., and McGraw R.: Threshold radar reflectivity for drizzling clouds, *Geophys. Res. Lett.*, 35, L03807, doi:[10.1029/2007GL031201](https://doi.org/10.1029/2007GL031201), 2008.
- Liu, D., Liu, Q., Liu, G., Wei, J., Deng, S., and Fu, Y.: Multiple Factors Explaining the Deficiency of Cloud Profiling Radar on Detecting Oceanic Warm Clouds, *J. Geophys. Res.-Atmos.*, 123, 8135–8158, 2018.
- 545 Mace, G. G., and Sassen K.: A constrained algorithm for retrieval of stratocumulus cloud properties using solar radiation, microwave radiometer, and millimeter cloud radar data, *J. Geophys. Res.*, **105**, 29,099–29,108, 2000.
- Mace, G. G., Zhang, Q., Vaughan, M., Marchand, R., Stephens, G., Trepte, C., and Winker, D.: A description of hydrometeor layer occurrence statistics derived from the first year of merged Cloudsat and CALIPSO data, *J. Geophys. Res.*, 114, D00A26, doi:[10.1029/2007JD009755](https://doi.org/10.1029/2007JD009755), 2009.
- 550 Marchand, R. T., Mace, G. G., and Ackerman, T. P.: Hydrometeor detection using CloudSat: An Earth orbiting 94 GHz cloud radar, *J. Atmos. Ocean. Tech.*, 25, 519–533, 2008.
- McLinden, M. L. W., Li, L., Heymsfield, G. M., Coon, M., and Emory, A.: The NASA GSFC 94-GHz Airborne Solid-State Cloud Radar System (CRS), *J. Atmos. Ocean. Tech.*, 38, 1001–1017, <https://doi.org/10.1175/JTECH-D-20-0127.1>, 2021. a

- Mühlbauer, A., McCoy, I. L., and Wood, R.: Climatology of stratocumulus cloud morphologies: microphysical properties and radiative effects, *Atmos. Chem. Phys.*, **14**, 6695–6716, <https://doi.org/10.5194/acp-14-6695-2014>, 2014.
- Mülmenstädt, J., Salzmann, M., Kay, J.E. *et al.* An underestimated negative cloud feedback from cloud lifetime changes. *Nat. Clim. Chang.* **11**, 508–513 (2021). <https://doi.org/10.1038/s41558-021-01038-1>
- Rapp, A. D., Lebsock, M., and L'Ecuyer, T.: Low cloud precipitation climatology in the southeastern Pacific marine stratocumulus region using CloudSat, *Environ. Res. Lett.*, **8**, 014027, <https://doi.org/10.1088/1748-9326/8/1/014027>, 2013.
- 560 Rémillard, J., Kollias, P., and Szyrmer, W.: Radar-radiometer retrievals of cloud number concentration and dispersion parameter in nondrizzling marine stratocumulus, *Atmos. Meas. Tech.*, **6**, 1817–1828, <https://doi.org/10.5194/amt-6-1817-2013>, 2013.
- Sasikumar, S., Battaglia, A., Puigdomènech Treserras, B., and Kollias, P.: The Estimation of Path Integrated Attenuation for the EarthCARE Cloud Profiling Radar, EGUsphere [preprint], <https://doi.org/10.5194/egusphere-2025-3573>, 2025.
- 565 Seifert, A., and Beheng, K. D.: A double-moment parameterization for simulating autoconversion, accretion and selfcollection, *Atmos. Res.*, **59–60**, 265–281, 2001.
- Serpetzoglou, E., Albrecht, B. A., Kollias, P., and Fairall, C. W.: Boundary Layer, Cloud, and Drizzle Variability in the Southeast Pacific Stratocumulus Regime. *J. Climate*, **21**, 6191–6214, <https://doi.org/10.1175/2008JCLI2186.1>, 2008.
- Stephens, G. L., and Coauthors: THE CLOUDSAT MISSION AND THE A-TRAIN. *Bull. Amer. Meteor. Soc.*, **83**, 1771–
- 570 1790, <https://doi.org/10.1175/BAMS-83-12-1771>, 2002.
- Stephens, G., Winker, D., Pelon, J., Trepte, C., Vane, D., Yuhas, C., L'Ecuyer, T., and Lebsock M.: CloudSat and CALIPSO within the A-Train: Ten Years of Actively Observing the Earth System. *Bull. Amer. Meteor. Soc.*, **99**, 569–581, <https://doi.org/10.1175/BAMS-D-16-0324.1>, 2018.
- Stephens, G. L., L'Ecuyer, T., Forbes, R., Gettleman, A., Golaz, J.-C., Bodas-Salcedo, A., Suzuki, K., Gabriel, P., and
- 575 Haynes J.: Dreary state of precipitation in global models, *J. Geophys. Res.*, **115**, D24211, doi:10.1029/2010JD014532, 2010.
- Suzuki, K., Nakajima, T. Y., and Stephens, G. L.: Particle growth and drop collection efficiency of warm clouds as inferred from joint *CloudSat* and MODIS observations. *J. Atmos. Sci.*, **67**, 3019–3032, <https://doi.org/10.1175/2010JAS3463.1>, 2010.
- Takahashi, H., Suzuki, K., and Stephens, G. L.: Land–ocean differences in the warm rain formation process in satellite observations, ground-based observations, and model simulations. *Quart. J. Roy. Meteor. Soc.*, **143**, 1804–
- 580 1815, <https://doi.org/10.1002/qj.3042>, 2017.
- Tanelli, S., Durden, S. L., Im, E., Pak, K. S., Reinke, D. G., Partain, P., Haynes, J. M., and Marchand, R. T.: CloudSat's Cloud Profiling Radar after two years in orbit: Performance, calibration, and processing, *IEEE Trans. Geosci. Remote Sens.*, **46**(11), 3560–3573, doi:10.1109/TGRS.2008.2002030, 2008.
- Tripoli, G. J., and Cotton, W. R.: A numerical investigation of several factors contributing to the observed variable density of
- 585 deep convection over south Florida. *J. Appl. Meteor.*, 1037–1063, 1980.
- Vohl, O., S. K. Mitra, S. Wurzler, K. Diehl, and H. R. Pruppacher, 2007: Collision efficiencies empirically determined from laboratory investigations of collisional growth of small raindrops in a laminar flow field. *Atmos. Res.*, **85**, 120–125.

- Wang, Y., Chen, Y., Fu, Y., and Liu, G.: Identification of precipitation onset based on Cloudsat observations, *J. Quant. Spectrosc. Ra.*, 188, 142–147, <https://doi.org/10.1016/j.jqsrt.2016.06.028>, 2017.
- 590 Wang, J., and Geerts, B.: Identifying drizzle within marine stratus with W-band radar reflectivity, *Atmos. Res.*, **69**, 1–27, 2003.
- Wehr, T., Kubota, T., Tzeremes, G., Wallace, K., Nakatsuka, H., Ohno, Y., Koopman, R., Rusli, S., Kikuchi, M., Eisinger, M., Tanaka, T., Taga, M., Deghaye, P., Tomita, E., and Bernaerts, D.: The EarthCARE mission – science and system overview, *Atmos. Meas. Tech.*, 16, 3581–3608, <https://doi.org/10.5194/amt-16-3581-2023>, 2023.
- 595 Wood, R.: Drizzle in stratiform boundary layer clouds. Part II: Microphysical aspects. *J. Atmos. Sci.*, **62**, 3034–3050, 2005.
- Wood, R.: Stratocumulus clouds. *Mon. Wea. Rev.*, 140, 2373–2423, <https://doi.org/10.1175/MWR-D-11-00121.1>, 2012.
- Wood, R., T. L. Kubar, and D. L. Hartmann, 2009: Understanding the Importance of Microphysics and Macrophysics for Warm Rain in Marine Low Clouds. Part II: Heuristic Models of Rain Formation. *J. Atmos. Sci.*, **66**, 2973–2990, <https://doi.org/10.1175/2009JAS3072.1>.
- 600 Wood, R., D. Leon, M. Lebsock, J. Snider, and A. D. Clarke (2012), Precipitation driving of droplet concentration variability in marine low clouds, *J. Geophys. Res.*, 117, D19210, doi:10.1029/2012JD018305.
- Wu, P., Dong, X., Xi, B., Liu, Y., Thieman, M., and Minnis, P.: Effects of environment forcing on marine boundary layer cloud-drizzle processes. *Journal of Geophysical Research: Atmospheres*, 122, 4463–4478. <https://doi.org/10.1002/2016JD026326>, 2017.
- 605 Xu, Z., Mace, G. G., & Posselt, D. J. (2019). A method for assessing relative skill in retrieving cloud and precipitation properties in next generation cloud radar and radiometer orbiting observatories. *Journal of Atmospheric and Oceanic Technology*, 36, 2283–2306. <https://doi.org/10.1175/JTECH-D-18-0204.1>.
- Xu, Z., Kollias, P., Lebsock, M., Battaglia A., and Sasikumar S.: Assessing Uncertainty and Biases in Total Liquid Water Path Retrieved from W-, Ka- and G-band Radar/Radiometer Observations from Space. *J. Atmos. Ocean. Tech.*, *accepted pending minor revision*, 2025.
- 610 Yamaguchi, T., Feingold, G., and Kazil, J.: Stratocumulus to cumulus transition by drizzle. *Journal of Advances in Modeling Earth Systems*, 9, 2333–2349. <https://doi.org/10.1002/2017MS001104>, 2017.
- Yang, F., Luke, E. P., Kollias, P., Kostinski, A. B., and Vogelmann, A. M.: Scaling of drizzle virga depth with cloud thickness for marine stratocumulus clouds. *Geophysical Research Letters*, 45, 3746–3753. <https://doi.org/10.1029/2018GL077145>, 2018.
- 615 Zhu, Z., Kollias, P., Luke, E., and Yang, F.: New insights on the prevalence of drizzle in marine stratocumulus clouds based on a machine learning algorithm applied to radar Doppler spectra, *Atmos. Chem. Phys.*, 22, 7405–7416, <https://doi.org/10.5194/acp-22-7405-2022>, 2022.